Calculation of electronic transport coefficients of Ag and Au plasma

E. M. Apfelbaum*

Joint Institute for High Temperatures of the Russian Academy of Sciences, Izhorskaya Street 13, Building 2, Moscow 125412, Russia

(Received 30 August 2011; revised manuscript received 21 October 2011; published 29 December 2011)

The thermoelectric transport coefficients of silver and gold plasma have been calculated within the relaxation-time approximation. We considered temperatures of 10–100 kK and densities of $\rho \lesssim 1$ g/cm^3. The plasma composition was calculated using a corresponding system of coupled mass action laws, including the atom ionization up to +4. For momentum cross sections of electron-atom scattering we used the most accurate expressions available. The results of our modeling have been compared with other researchers' data whenever possible.

DOI: 10.1103/PhysRevE.84.066403 PACS number(s): 52.25.Fi, 52.27.Gr, 52.25.Jm

I. INTRODUCTION

The electronic transport coefficients of metals (conductivity, thermal conductivity, and thermopower) play an important role in both fundamental problems and applications. For instance, information about these coefficients is necessary to describe the wire explosion experiments, the interaction of laser (or particle) beams with metals, and phenomena in interiors of giant planets or white dwarfs [1,2]. During these processes a metal may reach a dense plasma state, i.e., $T \geqslant$ 10 kK, and densities less than normal (note that normal density here refers to the value at an ambient pressure of 1 atm and a temperature of 293.15 K). This is the area of supercritical fluid, which until recent times was inaccessible for measurements, excluding only the case of alkali metals; however, measurements for the plasma of nonalkali metals in this region, based on the wire explosion technique, have appeared during past two decades (see Refs. [3–6] and references therein). We should note that for thermal conductivity and thermopower there are still no published experimental data in the region (only conductivity is measured). Nevertheless, available measurements, together with progress in computer productivity, have stimulated recent theoretical calculations. Now theoretical and experimental investigations of these coefficients exist for many metals in a wide range of densities and temperatures [1–20].

The coefficients described in the preceding paragraph can be calculated by various approaches. The most advanced of them are *ab initio* simulations [5–7], which are constructed upon formally exact Kubo - Greenwood formulas. In the context of this technique, a metal is considered a two-component system consisting of degenerate electrons and classical positive ions. The Born-Oppenheimer approximation can be applied in this case, i.e., the density-functional theory (DFT) treats the electron subsystem for some fixed ionic configuration, while the movements of ions are described by molecular-dynamics (MD) simulations. There are several numerical codes implementing this approach [7]. Although *ab initio* simulations are possibly the most rigorous and advanced approach, they are not a panacea (at least presently). There are technical problems, specifically concerning the small number of particles participating in simulations. There are also unresolved questions in physics, such as the unknown exchange-correlation functional in DFT or ambiguity in the choice of pseudopotentials. Besides, the pseudopotential conception originates from the solid-state physics and, as a rule, they are constructed to describe the substance properties near the normal density. Thus additional problems can arise at relatively small densities (much lower than normal one) where different asymptotic theories are applicable. In this case, the small number of particles mentioned above makes MD simulations problematic as well.

Another group of approaches is based on average atom models (AAMs) or cell models [6,8,10–14]. These methods consider a substance divided into neutral cells, each containing Z electrons, centered on a nucleus of charge Z, where Z is the element number in the Periodic Table. The radius of each cell is taken to be the Wigner-Seitz radius, determined from the density and atomic weight. The electrons in the cell can be described by DFT or Hartree-Fock techniques [12], which result in the electron density or the electron wave functions. Two latter objects allow one to construct self-consistent ion-ion pseudopotentials [13]. Then Kubo-Greenwood or Ziman formalism can be applied to calculate the coefficients of interest [9,10,13]. This cell approach originates from Thomas-Fermi (TF) theory as well as from solid-state physics (see, for instance, Ref. [15]). The average charge of the cell (or average ion charge) $Z_{\rm ion}$ can be introduced within AAMs ($Z_{\rm ion} \leqslant Z$). This value allows us to divide all electrons into bound and free ones. The number of free electrons in a cell is $Z_{\rm ion}$, while other electrons ($Z - Z_{\rm ion}$) are localized at the central nucleus. The AAM approaches (starting from the TF model) are well suited for the situation when $Z_{\rm ion} > 1$, i.e., when the plasma is fully ionized. However, in the case of relatively low densities (and small temperatures) almost all electrons should be localized, so $Z_{\rm ion}$ should tend to zero; metallic gas should consist of atoms, which have a finite size, while the cell radius tends to infinity. Thus, at relatively low densities the problems can arise again, as in the case of *ab initio* simulations.

The next group of methods considers plasma as a many-component mixture of electrons, positive ions, and atoms [16]. These methods are referred to as the generalized chemical models (GCMs). Earlier this approach was applied to the calculation of transport coefficients and the composition for some metals [2,16–19] and noble gases [21–23]. It originates from the physics of weakly coupled plasma that has relatively low

*apfel_e@mail.ru

densities, contrary to AAMs and *ab initio* simulations. Within GCMs the free energy of a mixture (for a given mass density and temperature) can be minimized with respect to the concentrations of particles contained in the mixture. This produces a system of mass action law equations, making it possible to obtain the composition. Then, like in the case of AAMs, various methods can be applied to find the coefficients themselves. Below we will consider this approach in more detail. Initially this approach was applied to hydrogen plasma by Saha [24], who considered it a mixture of noninteracting electrons, protons, and atoms. One can see that at relatively low temperatures, when a substance is not fully ionized, this approach requires the definition of what an atom (or ion) is or how to divide free and bound electrons. Consequently, GCMs work well at relatively low densities, when such division is possible. In this case, various theories relying upon asymptotic expansions and Green's-function techniques are applicable. Then a rigorous description of the particle interaction is possible within these theories. Analytical expressions for free energy can be constructed [1,2]. However, when the density grows, the atoms can be ionized by pressure, so the expansions are no longer applicable. In this case, the expression describing the interaction can still be constructed (for instance, by means of an approximation of numerical simulation data); however, these expressions have no rigorous theoretical grounds, unlike the case of low densities. The problem in the theoretical study is the following. The analytical expressions for free energy at low densities can be presented as sums of separate contributions, i.e., ideal and nonideal. The latter can also be divided into terms originating from interactions of specific separate components in the mixture. For instance, it can be the charge-charge or neutral-charge interaction. However, when the density grows, the interaction increases as well. In this case, the spectrum of a separate electron can be continuous, but it is no longer free because of the interaction. This electron is also not bound, like in the case of an isolated atom. Thus, under high densities (or pressures), it is impossible to provide an unambiguous definition of what an atom or any other complex particle is. Consequently, it is impossible to unambiguously describe the interaction between separate groups of particles. In this case, there is no rigorous analytical expression for the free energy, depending explicitly on the concentration of every component. As a result, the application of the GCM approach is limited at increased densities. Nevertheless, for most plasma states achieved in measurements at $T \geqslant 10$ kK, this technique is still valid [16,19].

For a number of metals the transport coefficients and equations of state in the plasma region have already been studied by various approaches mentioned above. For almost all of these metals we also have the measurement data. For instance, in recent experiments [3] Al, Ti, Fe, Ni, Cu, Mo, Ta, and W plasmas were studied; however, among the noble metals, only copper has received appropriate attention in theory and measurements. For gold there are calculations of conductivity [5,13] at $T \leqslant 10$ eV and corresponding measurements [5]. There are also calculations of Au conductivity within the AAM at $T \geqslant 10$ eV [14]. For silver, to our knowledge, there are no published calculations or any measurements in the plasma region. (Of course, for Ag at liquid state, at $T \leqslant 5$ kK, we have measurement data for conductivity and the equation of state; see, for instance Ref. [25].)

Thus the aim of present work is the calculation of electron conductivity, thermal conductivity, and thermopower of Ag and Au plasmas at temperatures 10–100 kK. We have applied the GCM to calculate the composition of Ag and Au plasma. Then, to determine the coefficients themselves, we have used the relaxation-time approximation, which, as we will see below, requires knowledge of the momentum cross sections. It should be mentioned that some preliminary results (only on the conductivity) are contained in Ref. [26]. The present paper contains (besides thermal conductivity and thermopower) more extended data and additional conductivity calculations and analysis, which are absent in Ref. [26].

The paper is organized as follows. In the following section formulas for the calculation of the coefficients and the chemical compositions are presented. Section III contains a description of the results; we will also compare the present results with the available data of other authors. A summary will be given in Sec. IV.

II. THEORETICAL RELATIONS

A. Relaxation-time approximation

The general scheme of the investigations of transport coefficients follows from the kinetic equations and, in particular, from the famous Boltzmann equation [27]. The mixture of light electrons and different heavy particles, comprising partially ionized plasma, is an example of the so-called Lorentz gas (or plasma). (It is the substance where the mass of one kind of particle in a mixture is much smaller than the masses of other kinds). If one uses the kinetic equation with the distribution function f_e to describe the behavior of electrons, then for the case of Lorentz plasma, the Boltzmann collision integral (as well as some other collision integral) can be transformed into a much simpler nonintegral expression, which has the form [13,27]

$$\left(\frac{df_e}{dt}\right)_{St} = -\frac{f_e - f_{e0}}{\tau}, \tag{1}$$

where f_{e0} is the equilibrium distribution function and τ is the relaxation time. Correspondingly, Eq. (1) and its consequences are known as the relaxation-time approximation, τ approximation, or Bhatnagar-Gross-Krook (BGK) approximation [28,29]. The solution of the kinetic equation within the BGK approximation, in turn, gives rise to possibly the simplest expressions for the electron transport coefficients [19,23,29,30]. Since the derivations of the corresponding relations for the electrical conductivity σ, thermal conductivity κ, and thermopower S_t are presented in Refs. [27,29,30], here we give only the final formulas

$$\begin{aligned}
\sigma &= -\frac{2|e|^2\sqrt{2m_e}}{3\pi^2\hbar^3} I_{3/2}, \quad S_t = \frac{1}{|e|T}\left(\mu - \frac{I_{5/2}}{I_{3/2}}\right), \\
\kappa &= -\frac{2\sqrt{2m_e}}{3\pi^2\hbar^3 T}\left(-I_{7/2} + \frac{(I_{5/2})^2}{I_{3/2}}\right), \\
I_n &= \int_0^\infty \epsilon^n \tau(\epsilon) \frac{\partial f_0}{\partial \epsilon} d\epsilon, \\
f_0 &= \frac{1}{\exp\left(\frac{\epsilon-\mu}{k_B T}\right)+1}, \quad \tau^{-1} = \sum_s n_s A_{es}^m(\epsilon)\sqrt{\frac{2\epsilon}{m_e}}.
\end{aligned} \tag{2}$$

Here m_e is the electron mass, e is the electron charge, $\hbar$ is the Planck constant, k_B is the Boltzmann constant, T is the temperature (in degrees kelvin), $A^m_{es}(\epsilon)$ is the momentum cross section of electrons on heavy particles of type s (s includes ions and atoms; the indices a, e, and i below will refer to the atoms, electrons, and ions, respectively), ϵ is the electron energy, f_0 is the Fermi-Dirac distribution function [which corresponds to f_{e0} in Eq. (1)], n_s is the number density of heavy particles, n_e is the electron number density, and μ is the chemical potential of an ideal electron gas. The cross section $A^m_{es}(\epsilon)$ and the disappearance of the angular dependence are discussed in detail in Ref. [30]. The chemical potential μ can be calculated by means of a well-known relation [2,16,27]

$$n_e = \frac{\sqrt{2m_e k_B T}}{\pi\hbar} J_{1/2}\left(\frac{\mu}{k_b T}\right), \qquad J_n(x) = \int_0^\infty y^n [1+\exp(y-x)]^{-1} dy \tag{3}$$

where $J_n(x)$ is the Fermi integral [2].

We should note that initially the τ approximation was obtained for the Boltzmann collision integral [28], which is valid for dilute gas with a prevalence of pair collisions. Thus, there are more complicated and more exact theories, which account for the effects beyond the pair collisions. For instance, the application of the Zubarev relevant operator approach [16] allows one to obtain more general and rigorous expressions than Eq. (2). For our present goal, though, the relaxation-time approximation is sufficient.

Equations (2) take into account only the scattering of electrons on heavy particles, but not the collisions between the electrons. Reference [13] correctly notes that the electron-current operator commutes fully with the electron-electron interaction Hamiltonian [see Eq. (16) of Ref. [13]]. Consequently, electron-electron collisions do not contribute directly to Kubo-Greenwood formulas, where the conductivity is calculated via a current-current correlation (averaged over the equilibrium distribution function), but they do change the form of the nonequilibrium part of the single-particle distribution function [see Ref. [22(a)]]. Thus, if the conductivity is obtained via kinetic theory and, consequently, using this nonequilibrium part, then the electron-electron contribution should be included. A more detailed discussion about electron-electron contribution is presented in Ref. [22]. Within the relaxation-time approximation, the electron-electron contribution cannot be included directly due to the conservation of momentum. However, this approximation accounts only for the first term of the distribution function expansion. So it is possible to go beyond the first term to account for the electron-electron contribution. Then the contribution of the electron-electron collisions can be included by means of an additional factor, which was introduced by Spitzer and Härm [31] for a fully ionized two-component plasma. For conductivity [31], $\sigma \to \gamma_{ee}(Z_{\rm ion})\sigma$, where $Z_{\rm ion}$ is the ion charge. When $Z_{\rm ion} \to \infty$ the factor $\gamma \to 1$. This factor was generalized in Ref. [32] for classical statistics [below, this result is denoted by $\gamma^*(Z_{\rm ion})$]. For the case of a partially ionized plasma the effects of possible electron degeneracy were taken into account [2,30]. Here we use the result of Refs. [2,32], where a corresponding factor was included in the collision frequency:

$$\tau^{-1} = \left(n_a A^m_{ea} + \sum_j \gamma(Z_j) n_j A^m_{ej}\right)\sqrt{\frac{2\epsilon}{m_e}}, \qquad \gamma^*(Z_j) = \frac{3\pi}{32}\left(1 + \frac{153Z_j^2 + 509Z_j}{64Z_j^2 + 345Z_j + 288}\right), \qquad \gamma(Z_j) = \gamma^*(Z_j) - [1-\gamma^*(Z_j)]\frac{T_F}{\sqrt{T_F^2+T^2}}. \tag{4}$$

The index j relates to positive ions only, while the index a relates to the atomic component. The Fermi temperature T_F is expressed as $T_F = \hbar^2(3\pi n_e)^{2/3}/2m_e k_B$. As one can see, for fully degenerate electrons ($T/T_F \to 0$), $\gamma(Z_j) \to 1$.

Evidently, the application of Eqs. (2)–(4) requires knowledge of the momentum cross sections A^m_{es} and the chemical composition, i.e., n_i,n_a, and n_e. Below, we will describe how these values can be obtained.

B. Cross sections

In a many-component plasma one needs to consider electron-ion and electron-atom scattering. The electron-ion collisions under the conditions considered here can be treated using the Born approximation, which gives rise to a formula of Rutherford type for the electron-ion transport cross section, but with a modified Coulomb logarithm with maximum and minimum impact parameters to ensure convergence of the collision integral. The corresponding expression used in our calculations can be obtained by many ways [2,16]. Its final form is

$$A^m_{ei}(\epsilon) = \frac{\pi}{\epsilon^2}\left(\frac{Z_i e^2}{4\pi\epsilon_0}\right)^2 \Lambda, \qquad \Lambda = 0.5[\ln(1+b) - b/(1+b)], \quad b = 8m_e\epsilon r_D^2/\hbar^2, \tag{5}$$

where r_D is the usual Debye radius [2] and ϵ is the energy of projectile particle (electron).

Measurements of electron-atom momentum cross sections for metals were unavailable until recently. Consequently, some model potentials (as a rule, of polarization type) have been used to calculate this value [1,2,16,33]. At large distances the neutral-charge potential decreases as r^{-4}. Below, there are two examples of these model potentials: $U_{\rm PP}$ was used in Ref. [16] and $U_{\rm HW}$ was used in Ref. [1] (PP denotes polarization potential and HW denotes hard wall). They have the following form (in a.u.):

$$U_{\rm PP}(r) = -\frac{\alpha}{2\left(r^2 + r_0^2\right)^2}, \qquad U_{\rm HW}(r) = \begin{cases} -\frac{\alpha}{2r^4}, & r > r_{\rm HW} \\ +\infty, & r \leqslant r_{\rm HW}. \end{cases} \tag{6}$$

Here α is the atom polarizability, which is a known value (see, for instance, Ref. [34]). In Ref. [16] the expression for the core radius r_0 was $r_0^4 = \alpha/2Z$ a.u. ($Z = 79$ for Au and $Z = 47$ for Ag, with Z the element number in the Periodic Table). The hard-wall radius $r_{\rm HW}$ has been determined here by the requirement that the ground-state energy level for $U_{\rm HW}$ must equal the negative-ion energy of the corresponding atom ($I_{\rm Au-} = 2.308\,63$ eV and $I_{\rm Ag-} = 1.302$ eV [34]). The

TABLE I. Parameters for the potentials in Eq. (6).

Parameter	Ag	Au
α ($a^3_{\rm Bohr}$)	52.59	35.12
r_0 ($a_{\rm Bohr}$)	1.643	1.351
$r_{\rm HW}$ ($a_{\rm Bohr}$)	1.642	1.422

parameters α, r_0, and $r_{\rm HW}$ are listed in Table I. We should note that the present definitions of the parameters r_0 and $r_{\rm HW}$ are not the only ones possible. For instance, if an atom has no negative ion, one should find another way to determine $r_{\rm HW}$ (see Ref. [1]). So the parameters of the model potentials can add a source of possible errors.

In recent years, the phase shifts for a number of metals, including Ag, were measured [35]. The calculations have been carried out consistently with the experiments. These calculations were performed with a parameter-free complex optical potential (OP) [35–37], which also accounts for the polarization effects. However, the influence of core electrons is regarded within the density-functional theory, which is much more accurate than the simple approximation used in Eq. (6). Optical potential calculations are in good agreement with phase-shift measurement data. In Fig. 1 we present the elastic momentum cross sections for electron-atom scattering for Ag and Au. The cross sections A^m_{ea} for $U_{\rm PP}$ and $U_{\rm HW}$ potentials were calculated here with the widely used variable-phase approach [38]. One can see that the OP can describe the features in cross-section behavior that are lost when the simple potentials in Eq. (6) are applied. Consequently, in our calculations we used the cross sections obtained by means of the OP. We now discuss the composition calculations.

C. Plasma composition

As we mentioned in the introduction, we consider plasma consisting of neutral atoms (index a or 0), electrons and several kinds of positive ions. The GCM approach will be used to calculate the composition. We will take into account the ions up to charge +4. The particle densities n_i, n_a, and n_e follow the conditions of charge neutrality and the mass conservation at a given mass density ρ:

$$\sum_j j n_j = n_e, \quad j = 1,2,3,4,\ldots, \tag{7a}$$

$$m_a n_a + \sum_j m_j n_j + m_e n_e = \rho. \tag{7b}$$

Here m_s is the mass of corresponding sort of particles. The substitution of Eq. (7a) into Eq. (7b) removes n_e and changes the expression under the summation $m_j \to m_j + j m_e$. Regarding $m_e \ll m_a, m_i$ and $m_a \approx m_i$, Eq. (7b) is usually reduced to $n_a + n_1 + n_2 + \cdots = \rho/m_a$. Further, to determine the particle densities, it is necessary to find the free-energy F minimum subjected to the conditions in Eqs. (7), i.e., to find the constrained minimum [1,2]. Consequently, one should differentiate the corresponding Lagrange function with respect to the particle numbers N_a, N_e, and N_i. (The particle density n and the number of particles N are related as $n = N/V$, where V is the system volume.) By definition the derivative

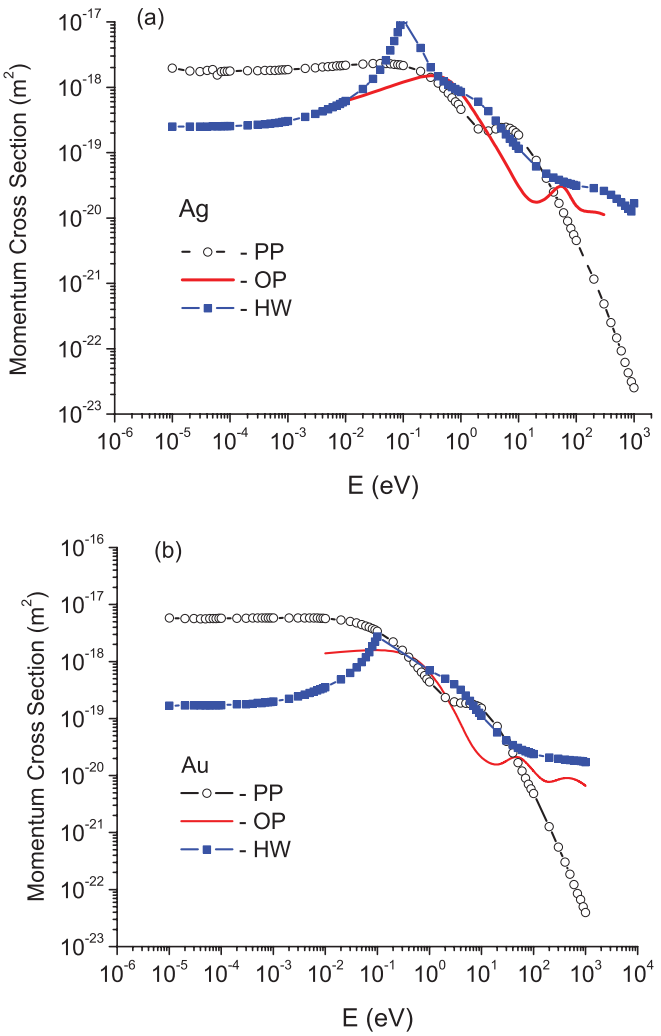

FIG. 1. (Color online) Comparison of electron-atom elastic momentum cross sections for different potentials. The lines with symbols denote potentials: the polarization potential (PP) (circles) and the hard-wall (HW) potential (squares) [Eq. (6)]. The solid line denotes the OP [36,37]. (a) Results for Ag. (b) Results for Au.

$\partial F/\partial N_s = \mu_s$, where μ_s is the chemical potential of the sth component. Thus, the resulting equations would describe the process of ionization and recombination [16]. Until now, we have not specified a particular form of F. Without loss of generality one can write $F = F_{\rm id} + F_{\rm int}$, where $F_{\rm id}$ is the free energy of noninteracting particles, while $F_{\rm int}$ is the interaction contribution. The ideal term $F_{\rm id}$ should include the interior partition functions of atoms and ions; however, the latter objects are divergent, therefore, some approximation is necessary for them. Below we will discuss this question in more detail. In Saha's work [24] only the $F_{\rm id}$ term was used. Thus subsequent generalizations, which have resulted in GCMs, intended to take into consideration the term $F_{\rm int}$ in the form of some explicit function of N_a, N_e, and N_i. This task was mentioned in the Introduction. It is clearly related to the problem of separation of the free and bound electronic states [1,2], so it has no unambiguous general solution, but some approximations are possible. Within GCMs it is supposed that $F_{\rm int}$ can be divided into different contributions as

follows [2,21,23]:

$$F(N_s,N_e,V,T) = F_{\rm id} + F_{\rm int} = F_{\rm id} + F_{\text{ch-ch}} + F_{N\text{-ch}}, \quad (8a)$$

$$\mu_s = \frac{\partial F}{\partial N_s} \Rightarrow \mu_{s+1} + \mu_e = \mu_s, \quad s = 0,1,2,\ldots. \quad (8b)$$

The index 0 relates to the atom. Equation (8b) gives a system of coupled mass action law equations, which are usually used to determine the composition [2]. Below, we will suppose that the heavy particles obey the classical statistics, while electrons can be degenerate. The ideal part of the free energy for classical particles is a sum of ideal free energies for separate components (denoted by index s), which are well-known values [2,21]:

$$F_{\rm id}(N_s,V,T) = k_B T N_s \ln\left(\frac{n_s\lambda^3}{Q_s e^*}\right), \quad \lambda = \frac{\sqrt{2\pi}\hbar}{\sqrt{m_s k_B T}}. \quad (9)$$

Here $e^* = 2.718\,28\cdots$ is the Euler number, Q_s is the interior partition function for the particle of type s (mentioned above), and λ is the de Broglie thermal wavelength [1,2]. For a degenerate system of noninteracting electrons the chemical potential is defined by the implicit equation (3). The other terms in Eqs. (8) are defined as follows: $F_{\text{ch-ch}}$ is the contribution due to the (charge-charge) interaction of charged species and $F_{N\text{-ch}}$ is the contribution due to the interaction of atoms with charged particles. The atom-atom contribution in metals is usually negligible [2,16] and will not be considered here. Various expressions for the respective contributions under consideration are possible [2,16,23]. The $F_{N\text{-ch}}$ contribution is usually described by means of the second virial coefficient approximation [2,16], i.e.,

$$V F_{N\text{-ch}} = 2k_B T N_a \sum_{s=i,e} B_{sa}(T) N_i, \quad (10)$$

where V is the volume and $B_{ia}(T)$ is the second virial coefficient. The latter was obtained here through a linearized Mayer function, like in Refs. [2,16], i.e., $B_{ia}(T) = \int U_{\rm PP}(r) d^3 r$. Here we used the polarization potential presented in Eq. (6). The interaction between the charges can be described by various approximated expressions. At low densities one of the most successful approximations [39] was obtained by means of a fugacity expansion within the grand canonical ensemble. For high densities it is possible to use Padé approximations [2,16]. In present calculations we have used the free energy $F_{\text{ch-ch}}$ offered in Ref. [40], which successfully connects both limits. Thus, substituting $F_{\rm id}$, $F_{N\text{-ch}}$, and $F_{N\text{-ch}}$ into Eqs. (8), we have the necessary expression for the free energy. Using Eq. (9), the particle densities can be obtained in explicit form [2]. Then Eqs. (7) and (8) can be transformed into the following system:

$$\begin{aligned} \frac{n_{s+1}}{n_s} &= \frac{Q_s^*}{Q_{s+1}^*}\exp\left[-\frac{1}{k_B T}[I_s - \Delta I_s + \mu_{\rm id}(n_e,T)]\right], \\ \Delta I_s &= \Delta\mu_s + \Delta\mu_e - \Delta\mu_{s+1}, \quad s = 0,1,2,\ldots \\ \Delta\mu_s &= \frac{\partial F_{\rm int}}{\partial N_s}, \quad \Delta\mu_e = \frac{\partial F_{\rm int}}{\partial N_e}, \\ n_0 + \sum_{s>0} n_s &= \rho/m_a, \quad \sum_{s>0} s n_s = n_e. \end{aligned} \quad (11)$$

Here $\mu_{\rm id}$ is defined by Eq. (3), I_s is the ionization potential (in the ground state) for the particle of type s, and ΔI_s is the decrease of the ionization potential due to the particle interaction. It is the system of Eqs. (11) that is usually solved to obtain n_s. The internal partition functions are $Q_s^* = Q_s \exp(E_{0s}/k_B T)$, where E_{0s} is the ground-state level energy for the particle of type s. The value Q_s for an isolated particle is defined as the sum over energies of the bound levels: $Q_s = Q_s(T) = \sum_j g_j \exp(-E_{js}/k_B T)$, where g_j shows the level degeneracy. As we mentioned above, this sum is divergent [1,2]. The divergence expresses the fact that the isolated particle is not a statistical system, so the conceptions of temperature and partition function are absent for it. However, real particles are always located in a substance; consequently their energy spectrum should be changed because of the particle interaction. In the first approximation it coincides with the spectrum of isolated particle, but it should be truncated at an energy level where the bound states cease to exist. Thus, only a finite number of levels is left. This truncation procedure has no unique implementation as far as it is again directly related to the separation of the free and bound states for a particle in a media. The latter task has no unambiguous solution, as we mentioned above. Nevertheless, there are several approaches to this problem. Some of them give rise to a density dependence in the partition function: $Q_s(T) \to Q_s(T,n_s)$. In this case the derivative $\partial Q_s(n_s)/\partial n_s$ should be added to ΔI_s. The corresponding correction can be important at low densities [41]; however, here we will use the Planck-Larkin procedure [1,2,41], which keeps Q_s density independent, i.e.,

$$Q_s \to Q_s^{\rm PL} = \sum_j g_j \left(\exp(-E_{js}/k_B T) - 1 + \frac{E_{js}}{k_B T}\right). \quad (12)$$

The set of energy levels E_{js} for atoms and singly ionized ions of Ag and Au studied here can be found in the National Institute of Standards and Technology electronic database [42]. The levels for higher ionized ions are presented in Ref. [43].

As we mentioned in the Introduction, the GCM approach has no rigorous theoretical grounds at higher density. Although the composition within the GCM can be formally calculated at any density and temperature, usually it gives correct results when the interparticle interaction is not too great [2,18]. Thus our calculations will be limited by some density $\rho_{\rm up}$ from above to ensure that the coupling parameter $\Gamma \sim e^2 n_e^{1/3}/k_B T \lesssim 1$. For instance, for Ag at $T = 10$ kK, $\rho_{\rm up} \sim 1$ g/cm^3. Evidently, at higher temperatures $\rho_{\rm up}$ increases; this question will be revisited later.

To characterize the plasma composition it is convenient to introduce the values [1,2,16,23]

$$\begin{aligned} \alpha_e &= \frac{n_e}{n_a + \sum_{s>0} n_s} \approx \frac{n_e m_a}{\rho}, \\ \alpha_s &= \frac{n_s}{n_a + \sum_{s>0} n_s} \approx \frac{n_s m_a}{\rho}, \quad s = 0,1,2,\ldots. \end{aligned} \quad (13)$$

The ionization degree α_e shows how many free electrons are generated per heavy particle, while the relative particle fraction α_s is the analogous value for a particle of type s. For two-component average atom models the average ion charge $Z_{\rm ion}$ also shows how many free electrons are generated per cell [5,13,18]. Thus it has the same physical meaning and we can compare α_e in GCMs and $Z_{\rm ion}$ in average atom models where available.

For Ag plasma there are no data about α_e, α_s, or $Z_{\rm ion}$ in GCMs, but there are results for $Z_{\rm ion}$ within the TF model [5,12,13]. We use the data on α_e for Ag plasma at isochor $\rho = 0.1\ \rho_n = 1.05\ {\rm g/cm^3}$ ($\rho_n = 10.5\ {\rm g/cm^3}$ is the normal density of silver) from Ref. [41(d)]. These data are presented in Fig. 2. In Fig. 2(a) the particle fractions of ions and atoms are presented at isochor $\rho = 1.05\ {\rm g/cm^3}$. At this relatively low density the ionization is caused mainly by temperature. Thus, the atoms dominate when $T \ll I_{\rm Ag} = 7.576\ 24\ {\rm eV} \approx 90\ {\rm kK}$ ($I_{\rm Ag}$ is the ionization potential of Ag atom). With temperature growth, the fraction of atoms decreases, while ionic fractions increase. At $T = 100\ {\rm kK}$ atoms nearly vanish and Ag^{2+} ions prevail. The fraction of Ag^{3+} is also non-negligible, but the fraction of Ag^{4+} is still indistinguishable from zero on the scale of Fig. 2(a). In Fig. 2(b) the ionization degrees α_e at the same isochor are presented according to different models. As one can expect in the models considered, α_e increases with

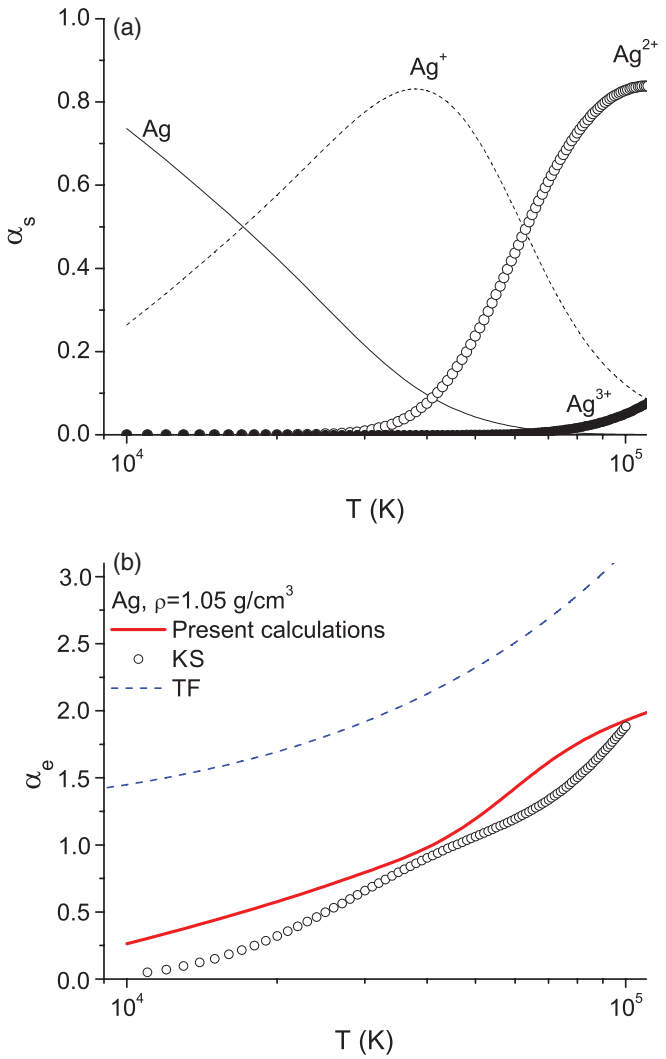

FIG. 2. (Color online) Composition of Ag plasma at isochor $\rho = 1.05\ {\rm g/cm^3}$ according to different models. (a) Relative fractions of ions and atoms in the present model. (b) Ionization degree α_e. Dashed lines denote results from the Thomas-Fermi model and circles denote the Khomkin-Shumikhin (KS) results from Ref. [41(d)].

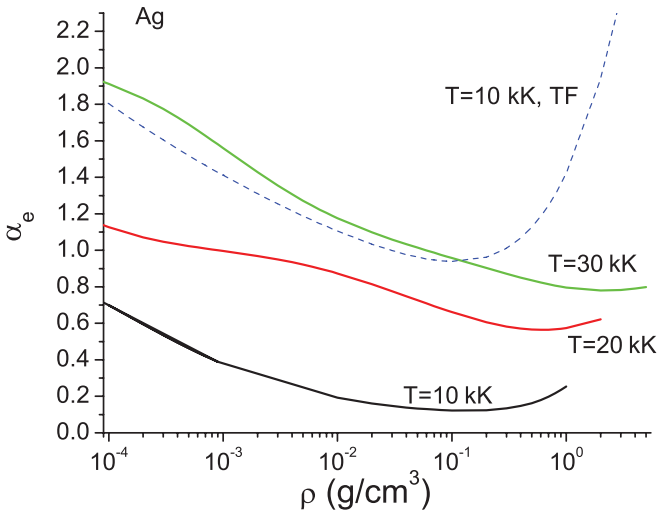

FIG. 3. (Color online) Ionization degree of Ag plasma at isotherms $T = 10$, 20, and 30 kK. The solid lines denote results from the present calculations and the dashed line denotes results from the TF model at $T = 10\ {\rm kK}$.

temperature. However, in the TF model, $Z_{\rm ion} > 1$ even at $T \approx 10\ {\rm kK}$, when the ionization is weak. This nonphysical behavior is especially evident at isotherms. The ionization degree at isotherms is presented in Fig. 3. Usually the ionization degree at isotherms for partially ionized plasma has a minimum at some point [16–23]. At isotherm $T = 10\ {\rm kK}$ this minimum is located near $0.1\ {\rm g/cm^3}$ in both our calculation and the TF model. Even at this point, though, the TF model gives $Z_{\rm ion} > 1$. Evidently, one needs an average atom model more advanced than the TF model to faithfully describe the variation of $Z_{\rm ion}$. For Au we can make a comparison with more advanced AAM approaches [13,14], but at higher temperatures: 5 and 10 eV. (In Ref. [14] only data at $T = 10\ {\rm eV}$ are present.) The corresponding results are presented in Fig. 4. At these temperatures Au plasma can be fully ionized as far as $I_{\rm Au} = 9.225\ 66\ {\rm eV} \sim T$. The parameter α_e (or $Z_{\rm ion}$) grows with density in all models. In Refs. [13,14], however, this growth is described by a very steep dependence, with an abrupt transition at normal density $\rho_n = 19.3\ {\rm g/cm^3}$. The growth leads to full ionization of s and d noble atom shells at $\rho > \rho_n$. The TF model yields a much smoother increase in $Z_{\rm ion}$. Our GCM model shows the lowest ionization degree with respect to the AAM approaches. It is noted that at $\rho \approx 0.8\rho_n$ the average charge in the Dharma-wardana (DW) model [13] at $T = 5\ {\rm eV}$ becomes greater than at $T = 10\ {\rm eV}$. There are no explanations for this behavior in Ref. [13], so it can only be ascribed to a model artifact. We should mention that the average charge (or ionization degree) is not defined unambiguously and it is not measurable directly. Moreover, *ab initio* methods do not require the knowledge of the average charge. Thus there is no uniquely correct model for this value. However, from general physical considerations we know features typical of it, some of which have been mentioned above. For example, there is a region of moderate densities at low temperatures (much lower than the atom ionization potential) where $Z_{\rm ion} < 1$. The GCMs, including the present calculations, demonstrate this behavior. The cell models usually have $Z_{\rm ion} > 1$ for all

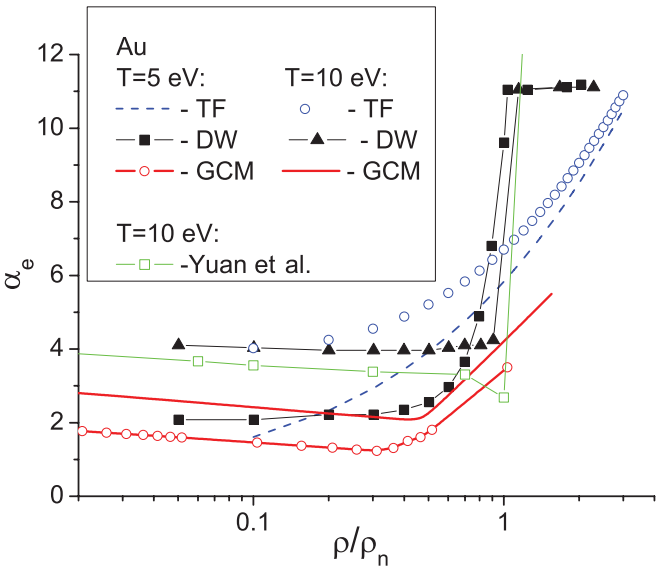

FIG. 4. (Color online) Ionization degree of Au plasma at isotherms $T = 5$ and 10 eV according to different models ($\rho_n = 19.3$ g/cm^3 is the normal Au density). GCM denotes results from the present calculations (red line corresponds to 5 eV and red line with open circles corresponds to 10 eV); DW denotes results of Dharma-wardana [13] (black line with solid squares corresponds to 5 eV and black line with solid triangles corresponds to 10 eV); and TF denotes results from the Thomas-Fermi model (blue dashed line corresponds to 5 eV and blue open circles corresponds to 10 eV). At $T = 10$ eV the results of Yuan *et al.* [14] are added (green line with open squares).

densities, which is the case for the TF and DW models considered here (see Fig. 1 of Ref. [13]). Thus, at low temperatures and moderate densities, the present composition model appears to provide better results. When the temperatures become higher (at the same moderate densities) to produce full ionization, it is difficult to say which kind of model is better. Under compression, however, the ionization is influenced by the interparticle interaction. At elevated densities the latter is better described in cell models. Consequently, at $\rho \sim \rho_n$ the cell models appear to be more physical, in particular, the DW model (of course, if the above-mentioned artifact can be explained or removed). Therefore, relying on the α_e behavior only, we cannot choose which kind of model is preferable for all the density ranges. Additional study is necessary with other values such as conductivity. Evidently, a different ionization description in the considered models results in different behavior of the conductivity (and other coefficients), as we will see in the following section.

III. RESULTS

A. Conductivity

First we present the results of the calculation for the conductivity. Although for Ag plasma we have no data for transport coefficients, we can use the compositions at $\rho = 1.05$ g/cm^3, according to the GCM [41] (see the preceding section) to calculate the conductivity at this isochor within the τ approximation. In Fig. 5 the corresponding data are presented at isotherms $T = 10$, 15, and 20 kK and at the

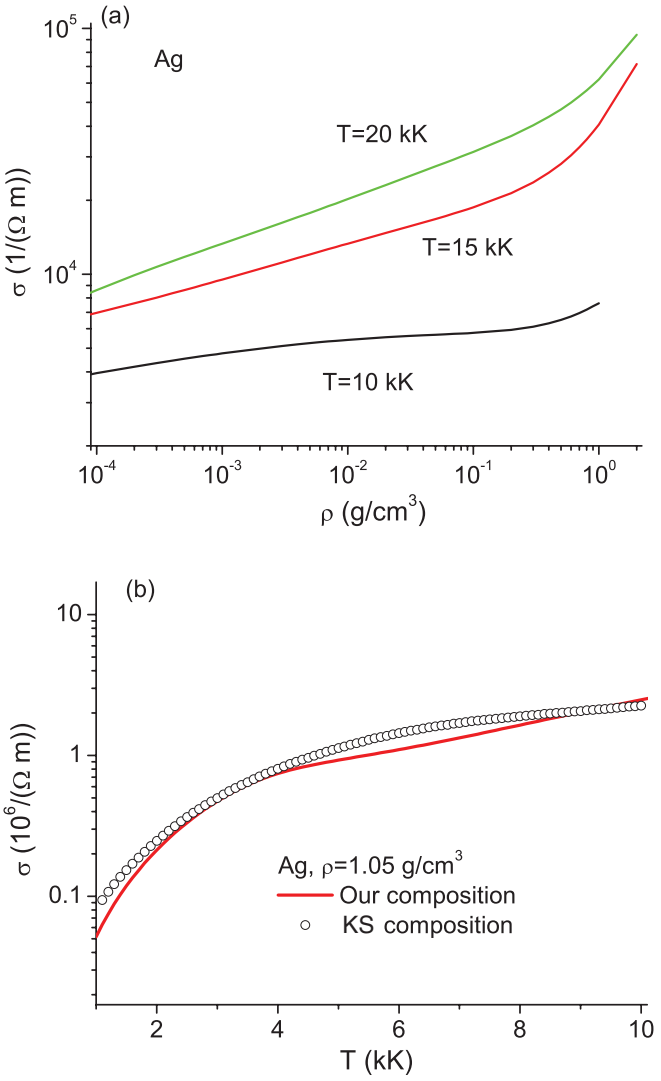

FIG. 5. (Color online) (a) Conductivity of Ag plasma at isotherms $T = 10$, 15, and 20 kK. (b) Conductivity of Ag plasma at isochor $\rho = 1.05$ g/cm^3. KS denotes the result of our calculation with composition of the model [41] (see the text).

isochor $\rho = 1.05$ g/cm^3. The conductivities, calculated with both compositions at the isochor, show close results, which is not surprising as variants of the GCM have been used in both cases. The coupling parameter $\Gamma \sim e^2 n_e^{1/3}/k_B T \lesssim 1$ along the isochor, while the degeneracy parameter [see Eq. (4)] $T_F/T < 0.1$; however, at the lowest isotherm ($T = 10$ kK) $\Gamma \sim 2$ and $T_F/T \sim 0.4$ at 1 g/cm^3. These values may indicate some limits of applicability for our calculations for Ag plasma within the considered model. Unfortunately, we cannot estimate the applicability of the present model from a comparison with any other data because the latter are absent. Here, though, the electron-atom contribution is described within the second virial coefficient approximation in Eq. (10). This approximation is applicable when its contribution to the pressure is much smaller (or at least smaller) than the ideal gas pressure, i.e., $A_{\text{virial}} \equiv 2B_{sa} n_a n_s/(n_a + n_s) \ll 1$. For the case in which atoms exist in plasma, i.e., when the temperature is sufficiently lower (much less than the atom ionization potential), this relation can be checked. For isotherm $T = 10$ kK

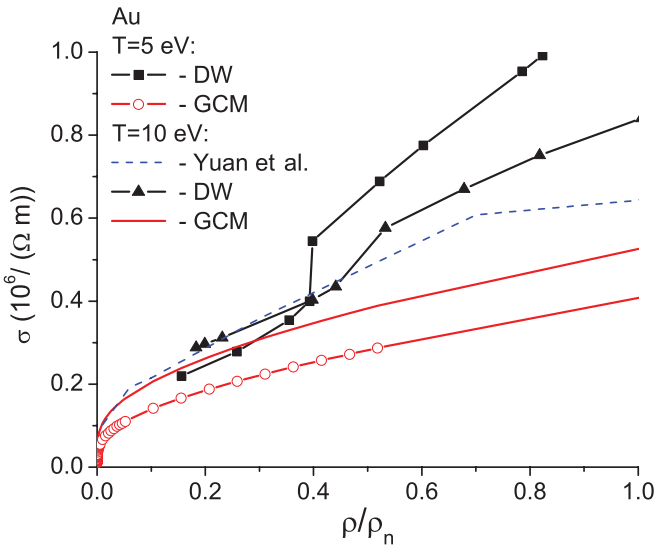

FIG. 6. (Color online) Conductivity of Au plasma at isotherms $T = 5$ and 10 eV. GCM denotes results from the present calculations, DW denotes results from Ref. [13], and Yuan *et al.* denotes results from Ref. [14].

at $\rho = 1$ g/cm^3, $A_{\text{virial}} = 0.33$ and at $\rho = 1.5$ g/cm^3, $A_{\text{virial}} = 0.73$. Thus the violation of the condition $A_{\text{virial}} \ll 1$ at $\rho \geqslant 1$ g/cm^3 at this density value can additionally indicate the limit of applicability (at least at $T = 10$ kK).

For Au plasma there are conductivity data calculated in Refs. [13,14]. In Fig. 6 these calculations, together with our results, are presented at the isotherms $T = 5$ and 10 eV. One could see that the model [13] shows the change in conductivity behavior at $\rho \sim 0.4\rho_n$ and $\rho_n = 19.3$ g/cm^3. Up to this density the conductivity in both models increases with temperature. Moreover, at $T = 10$ eV our calculations are in good agreement with the data of Ref. [14] when $\rho \leqslant 0.2\rho_n$. This trend usually corresponds to the plasmalike behavior. At higher densities, however, the conductivity in the model [13] decreases with temperature, like in liquid metals.

We should note that the steep increase in conductivity and change of its temperature dependence can be associated with the so-called dielectric-metal transition [1,2]. This phenomenon for many metallic plasmas can be more clearly seen in experiments if the temperature is much lower than the ionization potential of the corresponding atom [3], say, $T =$ 10 kK for nonalkali metals. In this case, if initially a substance is at a point with minimum ionization, it has low conductivity corresponding to the dielectric value. Then the compression along the isotherm gives rise to quick ionization and growth of conductivity to the metallic values. This behavior, also known as pressure ionization, was observed in measurements [3,4] and can be described by various approaches as mentioned in the Introduction, including the GCM [16]. One could see the onset of the pressure ionization in Fig. 3 at $\rho > 0.1$ g/cm^3 for Ag plasma and in Fig. 4 at $\rho > 0.4\rho_n$ for Au plasma. In addition to the increase in ionization, the character of the conductivity dependence on the temperature also should be changed, like in the AAM results of Ref. [13] in Fig. 6. This change is provided by the model of conduction itself, as well as the composition. The relaxation-time approximation used here cannot reproduce it. To obtain liquidlike behavior it is necessary to introduce the ion-ion correlations in the effective time τ by means of the structure factor [15]; alternatively, it would be better to calculate not the average time $\langle\tau\rangle$ but the inverse value $\langle 1/\tau\rangle$, like in the extended Ziman formula [13,14]. [More details about the extended Ziman formula are presented in Ref. [13], Eqs. (12)–(14).] Thus, possibly $\rho \sim 0.4\rho_n$ is the upper limit of applicability of the present model for Au at these temperatures.

TABLE II. Conductivity and mean ionization for Au plasma at $\rho = 0.5$ g/cm^3: σ^* denotes the data from Ref. [5], σ denotes the data from our calculations, Z_{TFD} denotes the TFD mean ionization from Ref. [5], and α_e denotes our mean ionization.

T (kK)	σ^* [(Ω m)$^{-1}$]	σ [(Ω m)$^{-1}$]	Z_{TFD}	α_e
15.0	0.98×10^4	1.11×10^4	0.46	0.23
20.0	2.38×10^4	2.48×10^4	0.66	0.46
25.0	3.81×10^4	3.95×10^4	0.85	0.66
30.0	5.03×10^4	5.52×10^4	1.02	0.82

In addition to the data of Refs. [13,14], the conductivity of Au plasma was measured in Ref. [5] at $\rho = 0.5$ g/cm^3, which corresponds to $0.026\rho_n$. At this density, our model should be applicable. Unfortunately, the experiments allow one to determine the internal energy, while the temperature cannot be obtained from the measurements directly. However, together with the measurements, *ab initio* simulations have been carried out in Ref. [5], where there are also the estimates of Z_{ion} according to different models, including the Thomas-Fermi-Dirac (TFD) model. In Table II we present the corresponding data on the conductivity and average charge. One can see that conductivities in both models are in good agreement.

One more way to validate the current approach is to consider another noble metal: Cu. For Cu there are measurements and calculations of conductivity in Ref. [6] together with an estimation of the mean ionization $\langle Z\rangle$, analogous to that ones in Ref. [5] for Au. These measurements have also been carried out at the isochor $\rho = 0.5$ g/cm^3. Unfortunately, we have no data for the OP momentum cross section for Cu; however, we can use the potential U_{PP} from Eq. (6) with our GCM (its parameters for Cu are $\alpha = 41.165a_{\text{Bohr}}^3$ and $r_0 = 1.609a_{\text{Bohr}}$). In Table III a comparison of our calculations for Cu with the data of Ref. [6] is presented. For Cu the difference in conductivity from the data of Ref. [6] is greater than in case of Au, but it can be explained by an inexact cross section.

TABLE III. Conductivity and mean ionization for Cu plasma at $\rho = 0.5$ g/cm^3: σ^* denotes the data from Ref. [6], σ denotes data from our calculations, $\langle Z\rangle$ denotes the mean ionization from Ref. [6], and α_e denotes our mean ionization.

T (kK)	σ^* [(Ω m)$^{-1}$]	σ [(Ω m)$^{-1}$]	$\langle Z\rangle$	α_e
10.0	1.00×10^4	3.22×10^3	0.10	0.05
15.0	2.00×10^4	1.17×10^4	0.21	0.18
20.0	3.10×10^4	2.42×10^4	0.32	0.30
25.0	5.40×10^4	4.06×10^4	0.58	0.52
30.0	7.00×10^4	6.01×10^4	0.73	0.70

B. Thermal conductivity and thermopower

For two other thermoelectrical coefficients (thermal conductivity κ and thermopower S_t) there are no data in the plasma region for either Ag and Au, so here we can discuss only our results. In Fig. 7(a) the thermal conductivity is presented at isotherms $T = 10$, 20, and 50 kK. Its behavior is similar to the trends in conductivity. At $T = 10$ and 20 kK gold plasma is more ionized than the silver plasma, so its thermal conductivity is a little higher. At $T = 50$ kK we have the opposite situation. We should note that the definition of thermopower considered here [see Eq. (2)] is not the only one possible. Phenomenological electric and heat currents consist of different contributions due to various inhomogeneities [27]. Each of the thermoelectric coefficients corresponds to some inhomogeneity. For instance, electrical conductivity describes the contribution due to the external field (in our case, it is an electric field), while two other coefficients describe the contribution due to the temperature gradient, which results in the appearance of the chemical potential gradient, which can be interpreted as an inhomogeneity in the chemical composition. The corresponding contribution can be separated into an additional term or it can be included in other contributions.

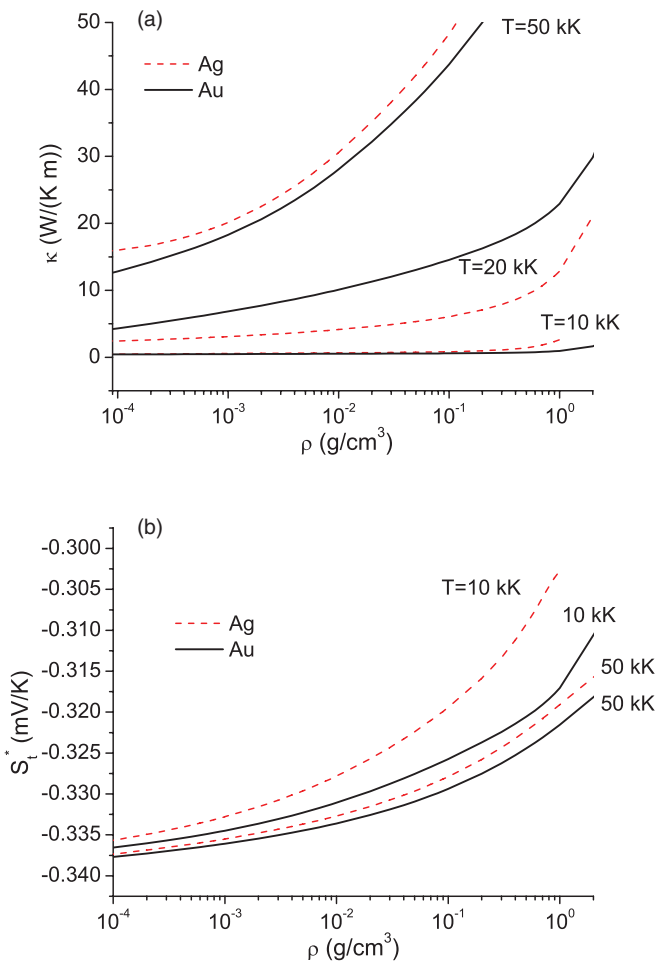

FIG. 7. (Color online) (a) Thermal conductivity of Ag (dashed lines) and Au (solid lines) plasma at isotherms $T = 10$, 20, and 50 kK. (b) Thermopower of Ag (dashed lines) and Au (solid lines) plasma at isotherms $T = 10$ and 50 kK.

For the latter case the definition of S_t in Eq. (2) should be modified as $S_t^* = S_t - \mu/eT$. A similar modification has been done, for instance, in Ref. [16]. The value S_t^* is presented in Fig. 7(b) for two isotherms $T = 10$ and 50 kK. We should note that in a fully ionized Lorentzian two-component plasma (without the electron-electron contribution) $S_t^* = -4k_B/e = -0.345$ mV/K [27]. In our case, as one could see in Fig. 7(b), $S_t^* \to -0.338$ mV/K at low density. There are two possible explanations for this difference. The first one is that the electron-electron contribution is not negligible at small densities in our model. The other is that the plasma has more than two components under these conditions. We should note that the growth of S_t^* with density also can indicate a nonmetal-to-metal transition, which is observed for conductivity (see Refs. [1,2,16]).

One more interesting question is how the Wiedemann-Franz relation is fulfilled for σ and κ. For degenerate electrons in liquid metals, when $T/T_F \to 0$, the experiments and theory show that σ and κ are connected as $\kappa = L\sigma T(k_B/e)^2$ [15,44], where the factor L, known as the Lorentz number, is constant $L \equiv L_0 = \pi^2/3 \approx 3.29$. At the opposite limit, when $T \to +\infty$ (a classical Lorentz plasma), this relation also holds. In this case, if electron-electron collisions are disregarded, $L = 4$ [27,29,31]. In partially ionized plasma, however, there can be atoms, which is different from the case for liquid metals or fully ionized weakly coupled plasma. Therefore, L is not necessarily constant. The calculations of L in partially ionized plasma for various metals have been presented previously, for instance, in Refs. [16,18]. If one considers the variation of L along some isotherm at $T \ll I$, where I is the ionization potential of the corresponding atom, the Lorentz number can be half $\pi^2/3$ if $\rho < \rho_n$ (ρ_n is the normal density). Although L increases and approaches L_0 if the density increases. The Ag and Au plasmas demonstrate analogous behavior. The Lorentz number varies from 1.4 to 3.29 for both metals, where the lowest value corresponds to the state with the lowest ionization.

IV. CONCLUSION

In this paper the electrical and thermal conductivity, as well as the thermopower, were calculated for silver and gold plasmas within the relaxation-time approximation. To describe electron-atom scattering we have used the most accurate presently available data for the momentum cross sections. The composition of the substance under consideration was obtained by means of a generalized chemical model. We have found that our model is applicable when the coupling constant $\Gamma \lesssim 1$. For this condition our results are in good agreement with the available data, obtained by other approaches for gold plasma. At higher densities our calculations of compositions show the onset of the pressure ionization, which is observed for various metal plasmas at relatively low temperatures. The τ approximation used here, however, does not give rise to the change of conductivity behavior from plasmalike to liquidlike, which should assist the process of ionization. Consequently, our model is limited by these densities. To get into the region of higher densities, it is necessary to use a more advanced transport model.

ACKNOWLEDGMENTS

The author thanks M. E. Povarnitsyn for helpful discussion and comments, V. I. Kelemen and E. Yu. Remeta for their data on the cross sections, and A. L. Khomkin and A. S. Shumikhin for the composition data. The work was supported by Russian Foundation for Basic Research Grant No. RFBR-12-008-00966.

[1] V. E. Fortov, I. T. Yakubov, and A. G. Khrapak, *Physics of Strongly Coupled Plasma* (Oxford University Press, Oxford, 2007).

[2] W. Ebeling, A. Förster, V. E. Fortov, V. K. Gryaznov, and A. Ya. Polishuk, *Thermophysical Properties of Hot Dense Plasmas* (Teubner Verlagsgesellshaft, Stuttgart, 1991).

[3] A. W. DeSilva and G. B. Vunni, Phys. Rev. E **83**, 037402 (2011); A. W. DeSilva and J. D. Katsouros, *ibid.* **57**, 5945 (1998).

[4] V. N. Korobenko and A. D. Rakhel, JETP **112**, 649 (2011); J. Clerouin, P. Noiret, V. N. Korobenko, and A. D. Rakhel, Phys. Rev. B **78**, 224203 (2008).

[5] P. Renaudin, V. Recoules, P. Noiret, and J. Clerouin, Phys. Rev. E **73**, 056403 (2006); J. Clerouin, V. Recoules, S. Mazevet, P. Noiret, and P. Renaudin, Phys. Rev. B **76**, 064204 (2007).

[6] J. Clerouin, C. Starrett, G. Faussurier, C. Blancard, P. Noiret, and P. Renaudin, Phys. Rev. E **82**, 046402 (2010); J. Clerouin, P. Renaudin, Y. Laudernet, P. Noiret, and M. P. Desjarlais, Phys. Rev. B **71**, 064203 (2005).

[7] A. E. Mattsson, P. A. Schultz, M. P. Desjarlais, T. R. Mattsson, and K. Leung, Model. Simul. Mater. Sci. Eng. **13**, R1 (2005).

[8] D. A. Liberman, Phys. Rev. B **20**, 4981 (1979).

[9] G. A. Rinker, Phys. Rev. A **37**, 1284 (1988).

[10] W. R. Johnson, A. C. Guetb, and G. F. Bertsch, J. Quant. Spectrosc. Radiat. Transfer **99**, 327 (2006); B. Wilson, V. Sonnad, P. Sterne, and W. Isaacs, *ibid.* **99**, 658 (2006); P. A. Sterne, S. B. Hansen, B. G. Wilson, and W. A. Isaacs, High Energy Density Phys. **3**, 278 (2007).

[11] C. Blancard and G. Faussurier, Phys. Rev. E **69**, 016409 (2004); G. Faussurier, C. Blancard, P. Cosse, and P. Renaudin, Phys. Plasmas **17**, 052707 (2010).

[12] A. F. Nikiforov, V. G. Novikov, and V. B. Uvarov, *Quantum-Statistical Models of Hot Dense Matter and Methods for Computation Opacity and Equation of State* (Birkhäuser, Boston, 2005).

[13] M. W. C. Dharma-wardana, Phys. Rev. E **73**, 036401 (2006).

[14] J. K. Yuan, Y. S. Sun, and S. T. Zheng, Phys. Rev. E **53**, 1059 (1996).

[15] J. M. Ziman, Adv. Phys. **13**, 89 (1964); **16**, 551 (1967).

[16] S. Kuhlbrodt and R. Redmer, Phys. Rev. E **62**, 7191 (2000); R. Redmer, *ibid.* **59**, 1073 (1999); S. Kuhlbrodt, B. Holst, and R. Redmer, Contrib. Plasma Phys. **45**, 73 (2005).

[17] E. M. Apfelbaum, J. Phys. A **39**, 4407 (2006); E. M. Apfelbaum and M. F. Ivanov, Plasma Phys. Rep. **27**, 76 (2001).

[18] E. M. Apfelbaum, High Temp. High Pressure **56**, 253 (2008).

[19] D.-K. Kim and I. Kim, Phys. Rev. E **68**, 056410 (2003); Contrib. Plasma Phys. **47**, 173 (2007).

[20] E. M. Apfelbaum, Phys. Chem. Liq. **48**, 534 (2010).

[21] Q. F. Chen, L. C. Cai, Y. J. Gu, and Y. Gu, Phys. Rev. E **79**, 016409 (2009).

[22] J. R. Adams, H. Reinholz, R. Redmer, V. B. Mintsev, N. S. Shilkin, and V. K. Gryaznov, Phys. Rev. E **76**, 036405 (2007); J. R. Adams, N. S. Shilkin, V. E. Fortov, V. K. Gryaznov, V. B. Mintsev, R. Redmer, H. Reinholz, and G. Röpke, Phys. Plasmas **14**, 052203 (2007).

[23] E. M. Apfelbaum, Contrib. Plasma Phys. **51**, 395 (2011).

[24] M. N. Saha, Proc. R. Soc. London Ser. A **99**, 135 (1921).

[25] C. Cagran, B. Wilthan, and G. Pottlacher, Thermochim. Acta **445**, 104110 (2006).

[26] E. M. Apfelbaum, Contrib. Plasma Phys. (to be published).

[27] E. M. Lifshitz and L. P. Pitaevskii, *Physical Kinetics. Course of Theoretical Physics*, Vol. 10 (Pergamon, Oxford, 2002).

[28] P. L. Bhatnagar, E. P. Gross, and M. Krook, Phys. Rev. **94**, 511 (1954).

[29] Y. T. Lee and R. M. More, Phys. Fluids **27**, 1273 (1984).

[30] W. A. Stygar, G. A. Gerdin, and D. L. Fehl, Phys. Rev. E **66**, 046417 (2002).

[31] L. Spitzer and R. Härm, Phys. Rev. **89**, 977 (1953).

[32] F. J. V. Van Odenhoven and P. P. J. M. Schram, Physica A **133**, 74 (1984).

[33] T. S. Ramazanov, K. N. Dzhumagulova, and M. T. Gabdullin, Phys. Plasmas **17**, 042703 (2010).

[34] A. A. Radtzig and B. M. Smirnov, *Parameters of Atom and Atomic Ions* (Energoatomizdat, Moscow, 1986).

[35] S. D. Tošić *et al.*, Nucl. Instrum. Methods Phys. Res. B **267**, 283 (2009).

[36] E. Yu. Remeta and V. I. Kelemen, J. Phys. B **43**, 045202 (2010).

[37] V. I. Kelemen, M. M. Dovnanych, and E. Yu. Remeta, Ukr. J. Phys. **55**, 1061 (2010).

[38] F. Calogero, *Variable Phase Approach to Potential Scattering* (Academic, New York, 1967).

[39] A. A Likalter, JETP **56**, 240 (1969).

[40] A. Y. Potekhin, G. Chabrier, and F. J. Rogers, Phys. Rev. E **79**, 016411 (2009); A. Y. Potekhin, G. Chabrier, A. I. Chugunov, H. E. DeWitt, and F. J. Rogers, *ibid.* **80**, 047401 (2009).

[41] A. L. Khomkin and A. S. Shumikhin, Eur. Phys. J. D **54**, 493 (2009); Plasma Phys. Rep. **34**, 251 (2008); A. L. Khomkin, V. S. Vorobev, I. A. Mulenko, and E. N. Oleinikova, *ibid.* **27**, 347 (2001); A. L. Khomkin and A. S. Shumikhin (unpublished).

[42] See http://physics.nist.gov/PhysRefData/ASD/levels_form.html.

[43] H. Benscopy, Y. N. Joshi, and Th. A. M. Vankleef, Can. J. Phys. **53**, 498 (1975); Th. A. M. VanKleef and Y. N. Joshi, *ibid.* **59**, 1930 (1981); Y. N. Joshi, A. J. J. Raassen, and A. A. van der Valk, J. Opt. Soc. Am. B **8**, 1372 (1991); J.-F. Wyart, Y. N. Joshi, L. Tchang-Brillet, and A. J. J. Raassen, Phys. Scr. **53**, 174 (1996).

[44] R. Brandt and G. Neuer, Int. J. Thermophys. **28**, 1429 (2007).